

ARPES Studies on Collapsed Tetragonal Phase Transition of  $\text{Ca}(\text{Fe}_{1-x}\text{Ph}_x)_2\text{As}_2$ 

Koji Tsubota<sup>1,2</sup>, Takanori Wakita<sup>1,2</sup>, Hiroki Nagao<sup>1,2</sup>, Chiaki Hiramatsu<sup>1,2</sup>,  
Toshihiko Ishiga<sup>1,2</sup>, Masanori Sunagawa<sup>1,2</sup>, Kanta Ono<sup>3</sup>, Hiroshi Kumigashira<sup>3</sup>, Masataka Danura<sup>1,4</sup>,  
Kazutaka Kudo<sup>1,4</sup>, Minoru Nohara<sup>1,4</sup>, Yuji Muraoka<sup>1,2</sup>, and Takayoshi Yokoya<sup>1,2\*</sup>

<sup>1</sup>The Graduate School of Natural Science and Technology, Okayama University, Okayama 700-8530, Japan

<sup>2</sup>Research Laboratory for Surface Science, Okayama University, Okayama 700-8530, Japan

<sup>3</sup>KEK, Photon Factory, Tsukuba, Ibaraki 305-0801, Japan

<sup>4</sup>Department of Physics, Okayama University, Okayama 700-8530, Japan

## 1 Introduction

The collapsed tetragonal (cT) phase is an interesting structural phase first observed in  $\text{CaFe}_2\text{As}_2$  under the application of pressure [1-4], and later observed in the chemical substitution of the As site [5], Fe site [6], or Ca site [7], in which  $T_c$  exceeding 40 K has been reported. The T-cT transition is characterized by the shrinkage in the  $c$ -direction by approximately 10% without breaking any symmetries, leading to changes in physical properties, such as electric resistivity and magnetic susceptibility [1-4,8-10]. The cT phase is nonmagnetic [2], in sharp contrast to the paramagnetism in the T phase. Although the absence or presence of superconductivity in the cT phase from pressure studies remains a controversial issue [8,10], systematic and detailed studies on As and Fe site substitution clearly demonstrate that the cT phase is nonsuperconductive [5,6]. In addition, the transport and magnetic properties shown a change from non-Fermi liquid behavior to Fermi liquid behavior across the T-cT transition [5,6]. Band structure calculations predicted the extinction of interband nesting between hole-like and electron-like cylindrical FS sheets around the center and corner of the Brillouin zone, respectively, in the cT phase [11-14]. Direct observation of the electronic structure of the T and cT phases can reveal the relationships between electronic structure and physical properties including superconductivity.

In spite of the interesting properties of the cT phase, the number of spectroscopic studies on the electronic structure of the phase has been limited. The FS topology of  $\text{CaFe}_2\text{As}_2$ , which is in the cT phase in ambient pressure, was reported from quantum oscillation experiments [15], which demonstrated the absence of a cylindrical sheet in

$\text{CaFe}_2\text{P}_2$ , in contrast to the FS topology observed for  $\text{CaFe}_2\text{As}_2$ . However, direct observation of the change in the FS topology across the transition by this technique for compounds with FeAs layers has not been reported, most probably due to the experimental difficulty under pressure. Although the FS topology and quasiparticle dispersions near  $E_F$  of many ironpnictides have been extensively studied by angle-resolved photoemission spectroscopy (ARPES), investigation of the cT phase by ARPES has not been reported so far.

In this letter, in order to understand the relationship of the change in electronic structure across the T-cT transition with the disappearance of superconductivity as well as with the change in physical properties, we have described ARPES on  $\text{Ca}(\text{Fe}_{1-x}\text{Ph}_x)_2\text{As}_2$  (Fig. 1). We observed a drastic change in the FS topology and band dispersion across the T-cT transition, which leads to the disappearance of hole-like cylindrical FS sheets around the zone center, while electron-like FS sheets at the X point remain nearly unchanged. The change in FS topology suppresses the interband nesting in the cT phase. Comparison between the present ARPES results and physical properties indicates strong correlations between the nesting of hole-like FS sheets at the zone center and electron-like sheets at the zone corner and physical properties including superconductivity. These data constitute the first experimental results on electronic structure across the T-cT transition.

## 2 Experiment

High-quality single crystals of  $\text{Ca}(\text{Fe}_{1-x}\text{Ph}_x)_2\text{As}_2$  with  $x=0.03$  were grown using a self-flux method [6]. Susceptibility measurements indicated a T-cT phase transition temperature of 70 K. ARPES were carried out at BL-28A of Photon Factory using circularly polarized light, using a VG-Scienta electron analyzer. In the measurements at BL-28A, the overall energy and angular resolutions were set to 15 meV and 0.1 deg, respectively. The crystals were cleaved *in situ* at  $T=30$  K and measured in vacuum at a base pressure better than  $1.5 \times 10^{-10}$  mbar. The calibration of the Fermi level ( $E_F$ ) of the samples was achieved by referring to that of gold.

## 3 Results and Discussion

In Fig. 2(a), an ARPES intensity map near  $E_F$  for  $\text{CaFe}_{0.97}\text{Rh}_{0.03}\text{As}_2$  at 100 K (T phase) obtained at

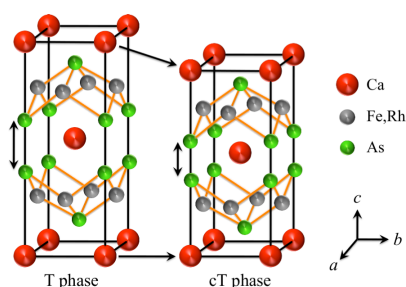


Fig.1: T- and cT-phase crystal structures of  $\text{CaFe}_2\text{As}_2$  (ThCr<sub>2</sub>Si<sub>2</sub>-type structure, space group  $I4/mmm$ ).

different photon energies (50-86 eV) is shown, together with the Brillouin zone for the body-centered tetragonal structure (red lines). In this plot, the ARPES intensity has been integrated over a range of  $\sim 15$  meV around  $E_F$ . We found that two strong-intensity regions are located symmetrically with respect to the high-symmetry point  $\Gamma$ , using an inner potential  $V_0$  of 14 eV. The FS shape is obscured by overlapping with this strong-intensity variation, which is probably due to the photon energy dependence of the photoelectron excitation cross section.

ARPES intensity plots as functions of binding energy and momentum along momentum cuts A and B [white arrows in Fig. 2(a)] are shown in Figs. 2(b) and 3(c), respectively. The blue filled and open circles represent peaks in the momentum distribution curves (MDCs) at different binding energies and in the energy distribution curves (EDCs) that are divided by the corresponding Fermi-Dirac distribution function, respectively. The superimposed lines are visual guides, representing band dispersions. While the top of the inner-hole band is located near  $E_F$ , the outer-hole band seems to cross  $E_F$ . Along cut B, the MDC at  $E_F$  shows two peak structures symmetric with respect to  $k=0$ , indicative of the  $E_F$  crossing of the bands. Along cut A, we found that the use

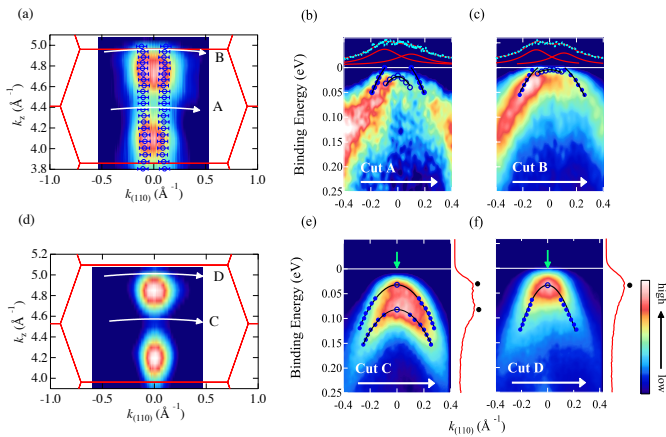


Fig. 2: (a) ARPES intensity map as functions of  $k_z$  and  $k_{(110)}$  at 100 K (T phase), which was made from photon-energy-dependent ARPES measurements ( $h\nu = 50-86$  eV) using an inner potential  $V_0$  of 14 eV. The red lines in (a) denote the Brillouin zone for the T-phase crystal structure with  $c = 11.4$  Å, while the blue circles indicate values of  $k_F$  from MDC analyses. (b) and (c) show ARPES intensity maps as functions of binding energy and  $k_{(110)}$  along cuts A and B in (a), respectively. Blue filled circles denote the peak positions in MDCs and curves superimposed on these circles are visual guides. Peak positions in normalized EDCs are also plotted with blue open circles. The light-blue dots at the top of (b) and (c) are the MDC at  $E_F$ , while the red curve superimposed on the MDC is the sum of the two Lorentzians used in MDC analyses. (d), (e) and (f) are the same as (a), (b), and (c), respectively, but at 30 K (cT phase). The curves shown on the right-hand side of (e) and (f) indicate the EDCs at  $k=0$  (green arrows).

of two components gives a better fit, suggesting the existence of two Fermi momenta  $k_F$ . Values of  $k_F$  that were determined from the analyses of the MDCs at  $E_F$  for different photon energies are shown by open circles in Fig. 2(a). The locations of the  $k_F$  indicate the existence of a nearly cylindrical FS along  $k_z$  in the T phase around the zone center. The observation of a hole-like cylindrical FS around the zone center is the same as that in previous ARPES on  $\text{CaFe}_2\text{As}_2$  under ambient pressure (T phase)[16,17].

In the cT phase, however, the electronic structure around the zone center is drastically modified. Figure 2(d) shows an ARPES intensity map near  $E_F$  of  $\text{CaFe}_{0.97}\text{Rh}_{0.03}\text{As}_2$  measured at 30 K plotted on the  $k_{(110)} - k_z$  plane. Although the intensity distribution showing two higher-intensity regions with respect to the  $\Gamma$  point in the cT phase is similar to that in the T phase, the energy locations of bands near  $E_F$  and consequently the FS topology are very different. In the cT phase, band dispersions at the  $\Gamma$  and Z points clearly show one hole-like and two hole-like bands near  $E_F$ , respectively, as shown in Figs. 2(e) and 2(f). The top of the hole-like band is located below  $E_F$  both along cut C and along cut D, as can be seen from the peak in EDC. This causes the cylindrical FS in the T phase to disappear in the cT phase. According to band calculations, the disappearance of the hole FS is closely related to the formation of As-As dimers (see Fig. 1).

In contrast to the drastic change in electronic structure across the T-cT transition around the zone center, the change around the zone corner is negligible. Figures 3(a) and 3(c) show band dispersions around the zone corner (X) in the T and cT phases, respectively. The band

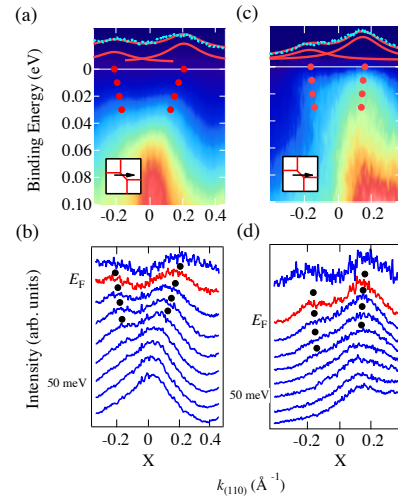


Fig. 3: (a) ARPES intensity map around the zone corner at 100 K (T phase) and (b) MDC at -10 to 70 meV binding energies at 50 meV intervals. The inset in (a) shows the measured location in the Brillouin zone. The light-blue dots at the top of (a) are the MDC at  $E_F$ , while the red curve superimposed on the MDC is the sum of the two Lorentzians used in MDC analyses. (c) and (d) are the same as (a) and (b), respectively, but at 30 K (cT phase). The filled circles indicate peak positions of MDCs.

dispersions in the T and cT phases appear slightly different, but the difference is due to the difference in the measured momentum space. Nonetheless, we observed one electron-like band in both phases, which can be seen more clearly in the MDCs [Figs. 3(b) and 3(d)].

From the ARPES results, we found that the T-cT transition removes the hole-like cylindrical FS around the zone center, while the electron-like band at the zone corner is relatively unchanged. The disappearance of the hole-like band has two major consequences that have great impact on the physical properties: reduction in the density of states (DOS) at  $E_F$  and loss of nesting. The reduction in the DOS at  $E_F$  can explain the sudden decrease in the magnetic susceptibility in the cT phase. In the cT phase, the electric resistivity also decreases. In our first approximation, the electric resistivity  $\rho$  is related to the mobility of carriers  $\mu$  and the number of carriers  $n$ .

$$1/\rho \propto \mu \times n$$

The decrease in the DOS at  $E_F$  leads to a decrease in the number of carriers, which increases resistivity. Contrary to our simple expectation, the electric resistivity in the cT phase decreases compared with that in the T phase. This suggests that the mobility  $\mu$  in the cT phase is larger than that in the T phase, which may be related to the presence and absence of nesting in the T and cT phases, respectively, as quasi-nesting causes more pronounced scattering. The change of nesting provides a microscopic interpretation of the recovery of the Fermi liquid behavior in the cT phases in  $\text{CaFe}_2(\text{As}_{1-x}\text{P}_x)_2$  [5] and  $\text{Ca}(\text{Fe}_{1-x}\text{Ph}_x)_2\text{As}_2$  [6]. According to the mechanism of superconductivity in iron-based superconductors, the quasi-nesting of hole and electron FSs connected with the AF vector, which can induce spin or orbital fluctuations, is the key to the exotic pairing mechanism [3,4,6,18]. Therefore the loss of nesting in non-superconductive cT compounds is consistent with these models. In contrast to that for alkali-metal doped iron-selenide superconductors, [19,20] the nesting of the electron-like FS at the zone corner in the cT phase for  $\text{Ca}(\text{Fe}_{1-x}\text{Ph}_x)_2\text{As}_2$  does not induce superconductivity.

#### 4. Conclusion

In summary, we examined the electronic structure of the T-cT phase transition using ARPES. The results show the disappearance of the hole-like cylindrical FS around the zone center across the transition, which gives rise to a decrease in the DOS at  $E_F$  and the reduction in the degree of nesting between a hole-like FS centered at the zone center and an electron-like FS centered at the zone corner.

The changes in physical properties across the transition and the absence of superconductivity in the cT phase can be related to the disappearance of the nesting in the cT phase. The data constitute the first experimental results on electronic structure across the T-cT transition.

#### Acknowledgements

We thank J. Sonoyama, T. Jabuchi, D. Yoshimura, N. Setoyama, and T. Okajima for assistance in PES measurements at PF or SAGA Light Source. We thank R. Yoshida and K. Okada for valuable discussions and suggestions. We also thank A. Ino for providing his ARPES analysis program. Experiments at SAGA Light Source and Photon Factory were approved by the Photon Factory Program Advisory Committee (Proposal No. 2011G086). This study was partially supported by JST-TRIP and a Grant-in-Aid for Scientific Research on Innovative Areas "Heavy Electrons" (No. 20102003) from the Ministry of Education, Culture, Sports, Science, and Technology of Japan (MEXT).

#### References

- [1] M. S. Torikachvili *et al.*, Phys. Rev. Lett. **101**, 057006 (2008).
- [2] A. Kreyssig *et al.*, Phys. Rev. B **78**, 184517 (2008).
- [3] A. I. Goldman *et al.*, Phys. Rev. B **79**, 024513 (2009).
- [4] D. K. Pratt *et al.*, Phys. Rev. B **79**, 060510 (2009).
- [5] S. Kasahara *et al.*, Phys. Rev. B **83**, 060505 (2011).
- [6] M. Danura *et al.*, J. Phys. Soc. Jpn. **80**, 103701 (2011).
- [7] S. R. Saha *et al.*, Phys. Rev. B **85**, 024525 (2012).
- [8] H. Lee *et al.*, Phys. Rev. B **80**, 024519 (2009).
- [9] J. R. Jeffries *et al.*, Phys. Rev. B **85**, 184501 (2012).
- [10] W. Yu *et al.*, Phys. Rev. B **79**, 020511 (2009).
- [11] T. Yildirim, Phys. Rev. Lett. **102**, 037003 (2009).
- [12] Y.-Z. Zhang *et al.*, Phys. Rev. B **80**, 094530 (2009).
- [13] D. A. Tompsett and G. G. Lonzarich, Physica B **405**, 2440 (2010).
- [14] M. Tomic *et al.*, Phys. Rev. B **85**, 094105 (2012).
- [15] A. I. Coldea *et al.*, Phys. Rev. Lett. **103**, 026404 (2009).
- [16] C. Liu *et al.*, Phys. Rev. Lett. **102**, 167004 (2009).
- [17] T. Kondo *et al.*, Phys. Rev. B **81**, 060507 (2010).
- [18] Y. Yanagi, Y. Yamakawa, and Y. Ono, Phys. Rev. B **81**, 054518 (2010).
- [19] Y. Zhang *et al.*, Nat. Mater. **10**, 2981 (2011).
- [20] T. Qian *et al.*, Phys. Rev. Lett. **106**, 187001 (2011).

\* yokoya@cc.okayama-u.ac.jp